Supplementary Information for:

Fluorination-assisted dealloying synthesis of porous rGO-FeF_2@C for high-performance lithium-ion battery and the exploration of its electrochemical mechanism

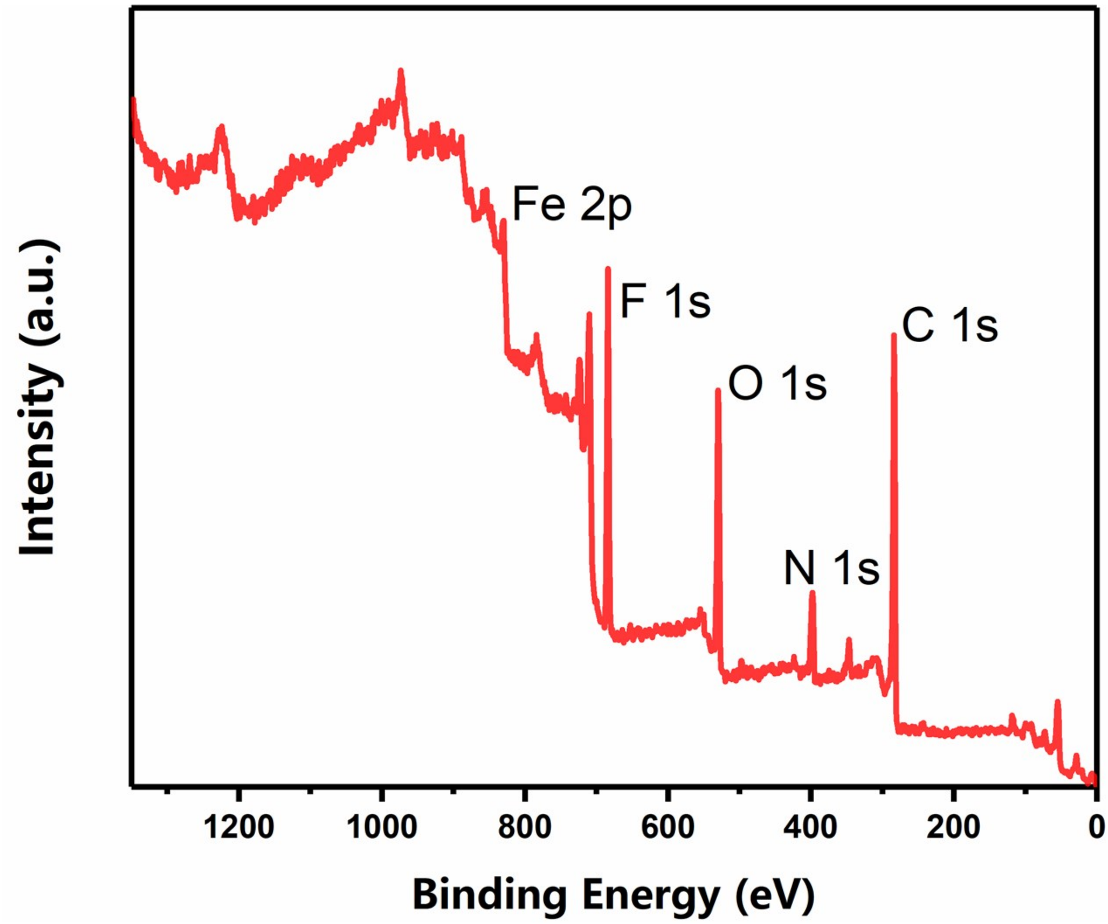

Fig. S1 The XPS survey spectrum of rGO-FeF_2@C

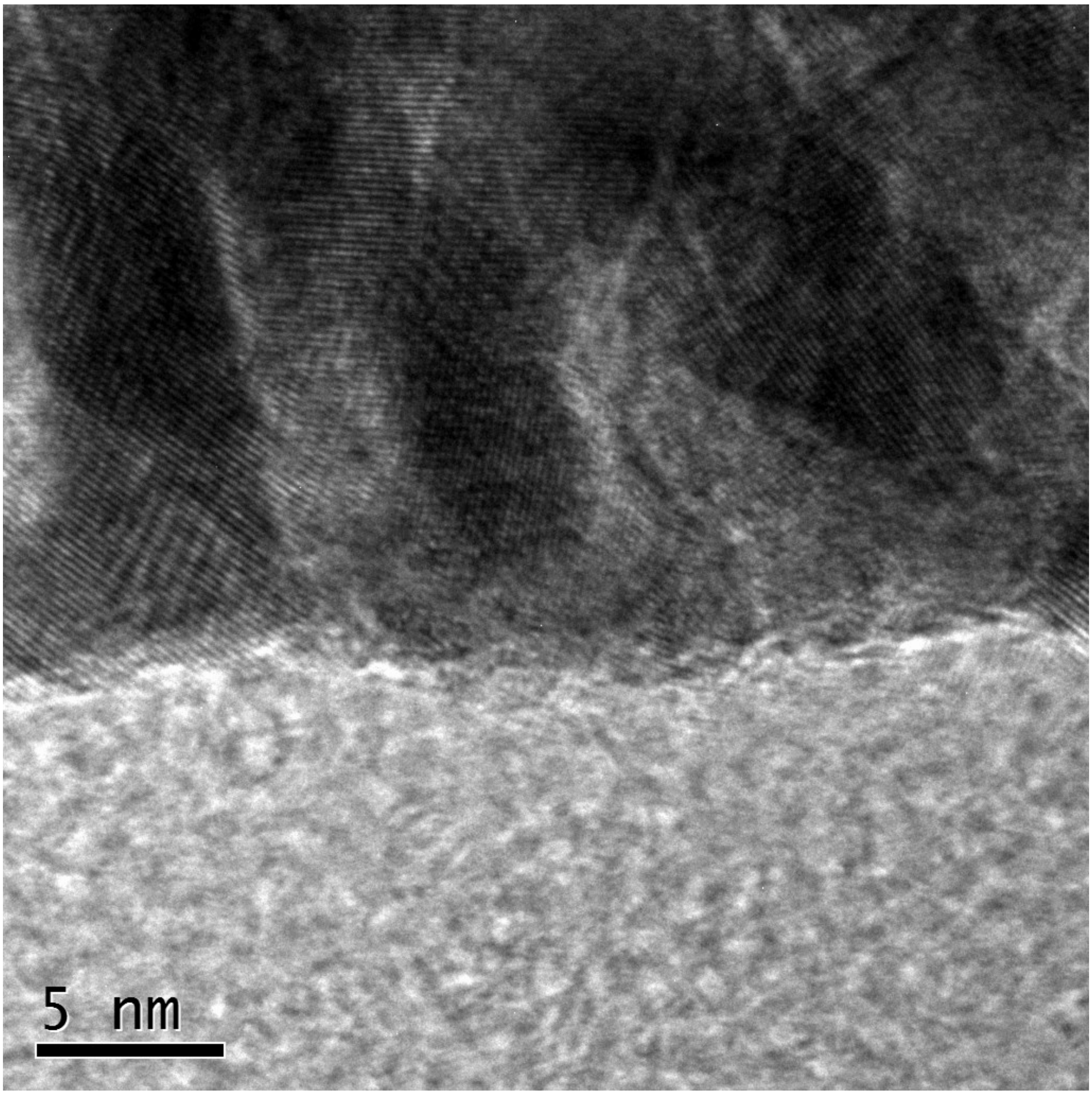

Fig. S2 The HRTEM image of P-FeF_2.

The confirmation experiment of the surface potential of FeF_2

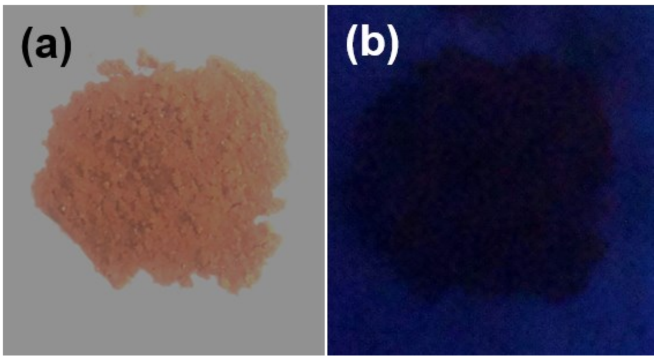

Fig. S3 The photograph of the fluorescein sodium powders under (a) visible light and (b) UV.

The experiments were conducted using a fluorescent-labeling method to explore the surface charge of the FeF_2. Fluorescein sodium was chosen as a fluorescent label. As anionic fluorescent molecule, the fluorescein sodium prefers to close to the positively charged substances. As be shown in Fig. 3(d), the fluorescein sodium/ethanol solution showed a yellow color in visible light and yellow-green fluorescence under UV-light. However, the dried fluorescein sodium powders didn't fluoresce under UV (Fig. S2). suggests that the fluorescein sodium shows fluorescence property in only the solvation environment. When FeF_2 was added to the fluorescein sodium /ethanol solution, the original yellow solution turns to colorless and transparent in visible and the fluorescence dims under UV-light. According to previously observed phenomena, we speculate that the fluorescein sodium molecules were adsorbed on the surface FeF_2 particles. Thus, the fluorescein sodium molecules lost their fluorescence property due to diverging from the solvation environment. This indicates that the FeF_2 surface is positively charged.

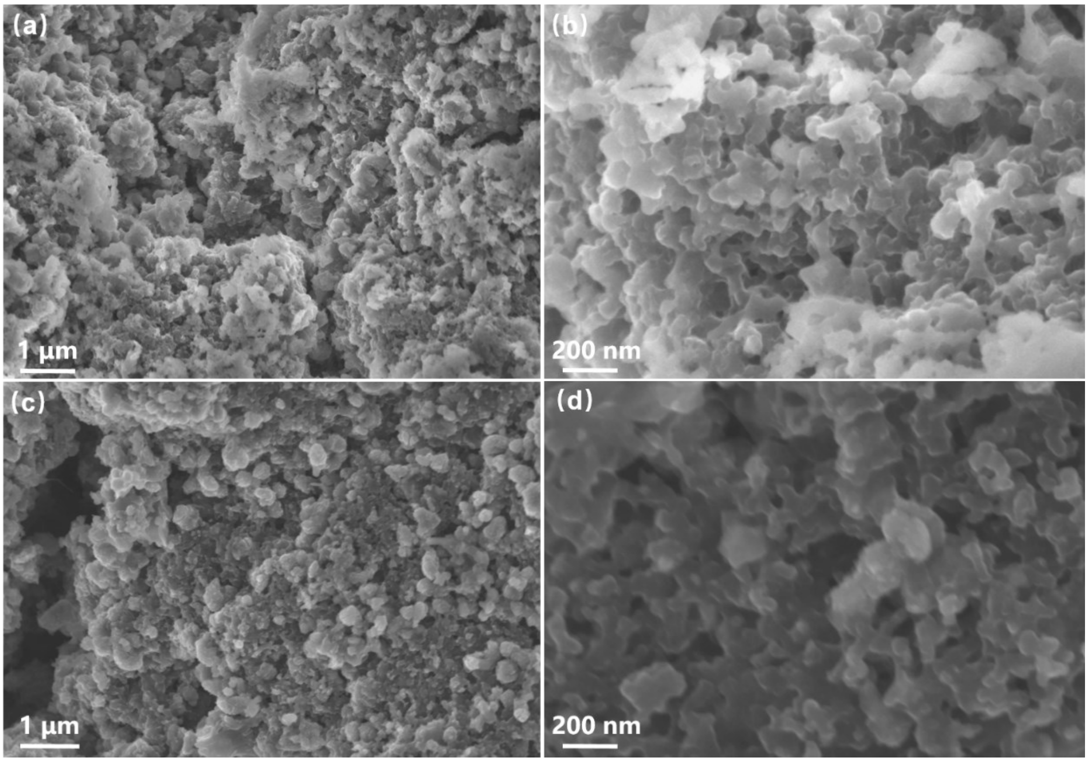

Fig. S4 SEM image of rGO-FeF_2@C after (a,b) 20 cycles and (c,d) 50 cycles.

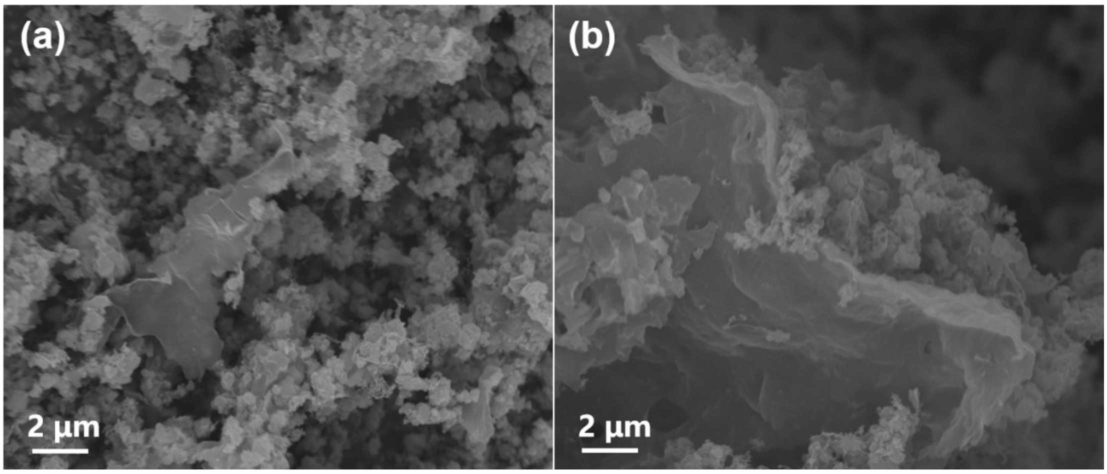

Fig. S5 (a) & (b) SEM image of rGO-FeF2@gluC.

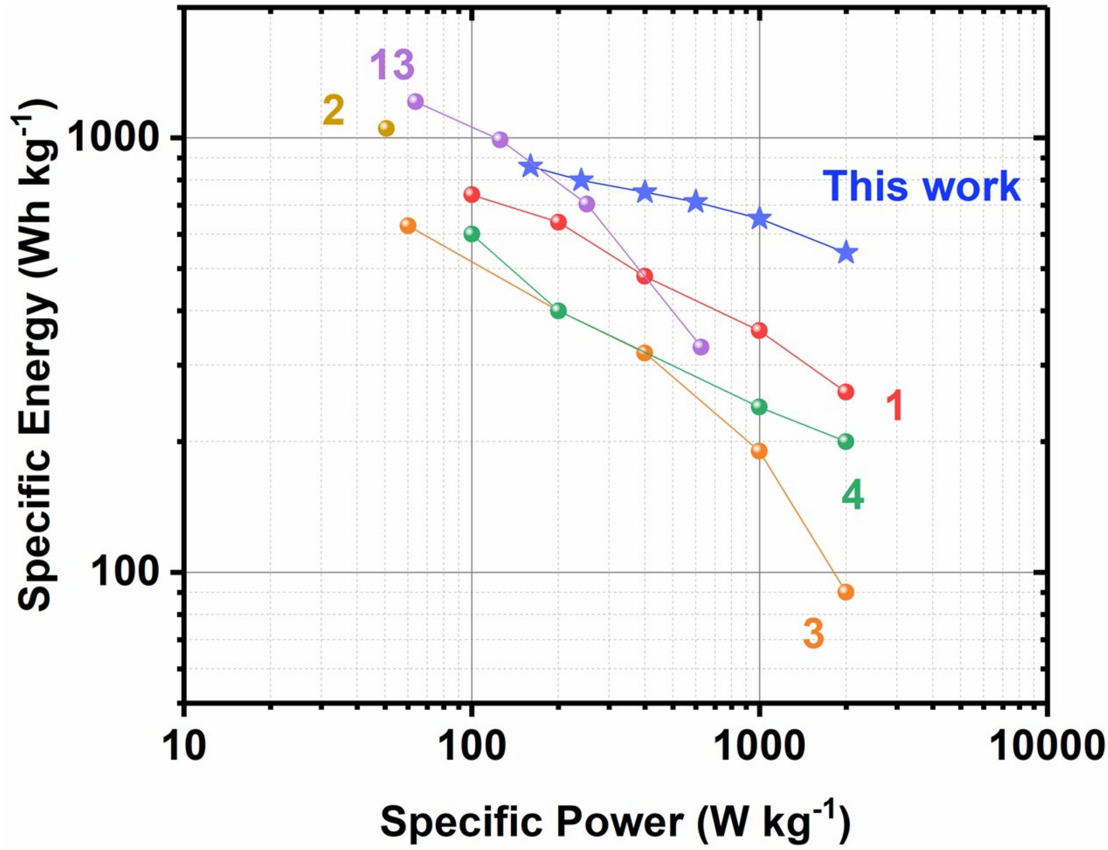

Fig. S6 Ragone plots of comparing with different literature in power density and energy density.

Tab. S1 Comparison of the electrochemical performance of the conversion type FeF_2 cathode materials.

materials	Current density	Voltage range	1st discharge capacity	Reversible capacity	Cycle number	Remaining capacity	Ref
$Ni@FeF_2@Al_2O_3$	200 mA g^{-1}	4.2-1.2 V	557 mAh g^{-1}	~400 mAh g^{-1}	50	250 mAh g^{-1}	1
BM-C$(FeF_2)_{0.55}$	22.7 mA g^{-1}	4.3-1.3 V	538 mAh g^{-1}	456 mAh g^{-1}	25	320 mAh g^{-1}	2
FeF_2–carbon core–shell	30 mA g^{-1}	4.3-1.3 V	345 mAh g^{-1}	314 mAh g^{-1}	50	217 mAh g^{-1}	3
FeF_2 nanorod/C	50 mA g^{-1}	4.2-1.0 V	352 mAh g^{-1}	263 mAh g^{-1}	50	263 mAh g^{-1}	4
	100 mA g^{-1}	4.2-1.0 V	345 mAh g^{-1}	221 mAh g^{-1}	50	181 mAh g^{-1}	
FeF_2	140 mA g^{-1}	4.0-1.0 V	-	~360 mAh g^{-1}	50	~200 mAh g^{-1}	5
FeF_2-rGO	200 mA g^{-1}	4.5-1.5 V	520 mAh g^{-1}	450 mAh g^{-1}	50	<100 mAh g^{-1}	6
FeF_2/C	60 mA g^{-1}	4.3-1.2 V	503 mAh g^{-1}	-	20	183 mAh g^{-1}	7
FeF2 film	12.5 mA g^{-1}	4.5-1.0 V	371 mAh g^{-1}	~330 mAh g^{-1}	10	348 mAh g^{-1}	8
C-FeF_2	20 mA g^{-1}	4.3-1.3 V	448 mAh g^{-1}	328 mAh g^{-1}	50	220 mAh g^{-1}	9
C-FeF_2	20 mA g^{-1}	4.3-1.3 V	418 mAh g^{-1}	363 mAh g^{-1}	40	297 mAh g^{-1}	10
C-FeF_2	20mA g^{-1}	4.3-1.3V	442 mAh g^{-1}	~420 mAh g^{-1}	50	~240 mAh g^{-1}	11
FeF_2	20 mA g^{-1}	5.0-1.0 V	590 mAh g^{-1}	420 mAh g^{-1}	25	200 mAh g^{-1}	12
rGO-FeF_2@C	200 mA g^{-1}	4.0-1.0 V	497 mAh g^{-1}	~400 mAh g^{-1}	50	~400mAh g^{-1}	This work
	200 mA g^{-1}		432 mAh g^{-1}	347 mAh g^{-1}		348 mAh g^{-1}	

References

1 S. Kim, J. Liu, K. Sun, J. Wang, S.J. Dillon, P.V. Braun, Improved performance

in FeF_2 conversion cathodes through use of a conductive 3D scaffold and Al_2O_3 ALD Coating, *Adv. Funct. Mater*., 2017, 1702783.

2 M.A. Reddy, B. Breitung, V.S.K. Chakravadhanula, C. Wall, M. Engel, C. Kübel, A.K. Powell, H. Hahn, M. Fichtner, CFx derived carbon–FeF_2 nanocomposites for reversible lithium storage ,*Adv. Energy Mater*., 2003, **3**, 308-313.

3 Y. Zhang, L Wang, J. Li, L. Wen, X. He, A one-pot approach towards FeF_2-carbon core-shell composite and its application in lithium ion batteries, *J. Alloys Compd*., 2014, **606**, 226-230.

4 J. Zhou, D Zhang, X. Zhang, H. Song, X. Chen, Carbon-nanotube-encapsulated FeF_2 nanorods for high-performance lithium-ion cathode materials, *ACS Appl. Mater. Interfaces*, 2014, **6**, 21223-21229.

5 Q. Huang, T.P. Pollard, X. Ren, D. Kim, A. Magasinski, O. Borodin, G. Yushin, Fading mechanisms and voltage hysteresis in FeF_2-NiF_2 solid solution cathodes for lithium and lithium-ion batteries, *Small*, 2019, **15**, 1804670.

6 D. Ni, W. Sun, C. Lu, Z. Wang, J. Qiao, H. Cai, C. Liu, K. Sun, Improved rate and cycling performance of FeF_2-rGO hybrid cathode with poly (acrylic acid) binder for sodium ion batteries, *J. Power Sources*, 2019, **413**, 449-458.

7 M. Tang, Z. Zhang, Z. Wang, J. Liu, H. Yan, J. Peng, L. Xu, S. Guo, S. Ju, G. Chen, Synthesis of FeF_2/carbon composite nanoparticle by one-pot solid state reaction as cathode material for lithium-ion battery, *J. Mater. Res. Technol*., 2018, **7**, 73-76.

8 M.F. Parkinson, J K. Ko, A. Halajko, S. Sanghvi, G.G. Amatucci, *Electrochim.*

Acta, 2014, **125**, 71-82.

9 M.A. Reddy, B. Breitung, C. Wall, S. Trivedi, V.S. Chakravadhanula, M. Helen, M. Fichtner, Effect of vertically structured porosity on electrochemical performance of FeF_2 films for lithium batteries, *Energy Technol.*, 2016, **4**, 201-211.

10 M. Helena, M. Fichtner, M.A. Reddy, Electrochemical synthesis of carbon-metal fluoride nanocomposites as cathode materials for lithium batteries, *Electrochem. Commun.*, 2020, **120** 106846.

11 M.A. Reddy, B. Breitung, V.S.K. Chakravadhanula, M. Helen, R. Witte, C. Rongeat, C. Kubel, H. Hahn, M. Fichtner, Facile synthesis of C-FeF_2 nanocomposites from CF_x: influence of carbon precursor on reversible lithium storage, *RSC Adv.*, 2018, **8**, 36802-36811.

12 M.J. Armstrong, A. Panneerselvam, C. O'Regan, M.A. Morris, J.D. Holmes, Supercritical-fluid synthesis of FeF_2 and CoF_2 Li-ion conversion materials, *J. Mater. Chem. A*, 2013, **1**, 10667-10676.

13 A.W. Xiao, H.J. Lee, I. Capone, A. Robertson, T.U. Wi, J. Fawdon, S. Wheeler, H.W. Lee, N. Grobert, M. Pasta, Understanding the conversion mechanism and performance of monodisperse FeF_2 nanocrystal cathodes, *Nat. Mater.*, 2020, **19**, 644-654.